Diffuse-interface effects near a cusp singularity on a free surface

L. M. Pismen
Department of Chemical Engineering and Minerva Center for Nonlinear Physics of Complex Systems, Technion–Israel Institute of Technology, 32000 Haifa, Israel
(Received 7 June 2004; published 17 November 2004)

Cusp singularity on a free surface of a viscous fluid driven by a vortex dipole is resolved through nanoscale molecular interactions. The cusp is formed at finite capillary number due to a decrease of surface tension caused by conjoining interaction near the cusp. The related effects of cusp geometry are weak Marangoni flow, vapor condensation, and a slight decrease of liquid density near the cusp creating a depletion tail downstream.

DOI: 10.1103/PhysRevE.70.051604 PACS number(s): 68.03.Cd, 47.15.Gf, 68.03.Fg, 05.70.Np

I. INTRODUCTION

Classical hydrodynamics is plagued by stress singularities linked to singularities of free surfaces. These singularities can be resolved only by modifying boundary conditions, either phenomenologically or through physical insight, e.g., by taking into account molecular interactions near the interfaces. A notorious example is flow near a three-phase contact line [1,2], where the physical models suggested to resolve the singularity range from activated flow in a first molecular layer [3,4] through interfacial relaxation [5] to diffuse interface theory [6–8].

A simpler but less known example is a cusp singularity on a free surface observed in flow induced by a vortex dipole [9]. An elegant two-dimensional (2D) solution based on conformal transformation was given by Jeong and Moffatt [10] and further extended tothe case of variable surface tension by Antanovskii [11]. It was found that a cusp singularity appears at $\mathrm{Ca}\to\infty$, where $\mathrm{Ca}=u_0\eta/\gamma_0$ is the capillary number based on the characteristic flow velocity u_0 (related to the dipole strength), dynamic viscosity η, and standard surface tension γ_0 of a flat quiescent interface. The stress becomes singular at the cusp tip. The singularity appearing asymptotically at vanishing surface tension would not be troublesome from the physical point of view, but for the extraordinary way it is approached. Although the curvature at the tip remains formally finite at any finite Ca, the curvature radius $\kappa^{-1}=\frac{256}{3}\exp(-32\pi\mathrm{Ca})$ goes below molecular scale already at $\mathrm{Ca}=O(10^{-1})$. Moreover, the cusp may appear already at finite Ca when surface tension vanishes at the cusp tip [11].

It must be noted that the formation of a cusp singularity is not a mere mathematical quirk, since it leads to a qualitative and physically significant change in flow pattern: a stagnation line on the free surface disappears, and free surface streamlines proceeddirectly into the fluid interior. Jeong and Moffatt [10] dismiss the question of what "really happens" near the tip as "philosophical," but it is indeed a physical question dependent on weak corrections to hydrodynamic theory, which become important only close to the singularity.

The additional factors coming into play near the singularity might be of either physical or hydrodynamic nature. The most straightforward correction remaining within hydrodynamic theory is taking into account finite viscosity of the gas phase treated by the original theory as inviscid, i.e., ignored altogether. Eggers [12] has resolved the interface profile numerically for small but finite viscosity ratios, and showed that the tip breaks, leading to air entrainment, way before approaching the cusped form or thinning to molecular dimensions.

A different path was taken earlier by Shikhmurzaev [13], who suggested resolving this singularity (as well as that at the contact line) by introducing in a phenomenological manner an interfacial layer treated as a separate phase. Advection of this layer along the interface causes changes of surface tension dependent nonlocally on the flow pattern and feeding back upon the flow through an analog of the Marangoni effect.

This paper continues the trend toward resolving a hydrodynamic singularity by introducing a more refined physical model on shorter scales. An interfacial layer of a finite (nanoscale) thickness appears in a natural way in diffuse interface theory going back to van der Waals [14]. The advantage of this theory is in a possibility to directly relate short-scale modifications of hydrodynamic theory to molecular interactions. The problem in question, where, unlike the contact line problem, a precise hydrodynamic solution exists, is a good testing ground for a more general challenge of resolving hydrodynamic singularities through molecular interactions.

Coupling diffuse interface theory to hydrodynamics involves modification of macroscopic hydrodynamic equations by including thermodynamic driving forces arising in a nonequilibrium fluid. This theory is essentially mesoscopic, and assumes linear coupling between fluxes and thermodynamic forces in the spirit of Onsager's nonequilibrium thermodynamics. Local mesoscopic hydrodynamic theory [15] modifies hydrodynamic equations by including in the stress balance a reversible part of the stress tensor, called the capillary tensor, which is derived from an applicable free energy functional. This theory fails, however, to incorporate kinetic retardation of interphase transport, as the only dissipation mechanism explicitly included in this theory is viscosity. Relaxation to the equilibrium density distribution in thin interfacial layers might be described, in the spirit of Cahn-Hilliard theory [16], by including diffusional fluxes driven by gradients of chemical potential. This, however, brings about conceptual difficulties, since diffusional and ad-

vective fluxes cannot be separated in a unique way in a one-component fluid.

The formidable task of formulating and solving coupled kinetic and hydrodynamic equations is relieved by a great disparity of scales. This allows one to separate the inner interfacial region where macroscopic flow velocity is constant and the interface is close to equilibrium, and the outer region where flow is incompressible, while weak gradients of chemical potential are relaxed by diffusion. Macroscopic flow driven by external sources will remain unaffected by gradients of chemical potential almost everywhere. Nevertheless, coupling to the inner region influences the flow through boundary conditions sensitive to changes of surface tension and interphase transport. The corrections, even minute, may become essential when the classical hydrodynamic solution is singular.

The peculiarity of the cusp is a drastically increasing aspect ratio at close approach to the tip; as a result, its width falls into the nanoscale range already at mesoscopic distances from the tip. This brings about several physical effects, which we shall consider in turn. First, the conjoining interaction of two interfaces at close approach changes the surface tension, which withers gradually to zero at the tip, as discussed in Sec. II. The hydrodynamic solution with variable surface tension is obtained using the conformal transformation technique [10,11] in Sec. III. In Sec. IV we turn attention to mass transport facilitated by shifts in equilibrium chemical potential, bringing about vapor condensation. This, in turn, facilitates removal of a neutral component (air) from the narrow gap by diffusion, thereby eliminating backflow and preventing pressure buildup in the narrow gap, as discussed in Sec. V. Diffusion on the background of the macroscopic flow manifests itself only in a weak density depletion downstream from the cusp tip.

II. SURFACE TENSION AND CONJOINING POTENTIAL

We consider first the effect of variable surface tension. As two interfaces approach one another, the overlap of the tails of the density profile causes a decrease of interfacial energy, i.e., surface tension, which must vanish at zero separation when the gas layer between the two liquid volumes disappears altogether. Thus, the dependence of surface tension on the separation h can be expressed as $\gamma=\gamma_0\chi(h)$, where $\chi(0)=0$ and $\chi(\infty)=1$. We shall see that the particular shape of this function affects only coefficients in the final expressions.

Consistent computation of the dependence $\chi(h)$ requires application of diffuse interface theory in the vicinity of the tip. The starting point [8,17] is the free energy functional written in the density functional approximation as

$$\mathcal{F}=\int \rho(\mathbf{x})F(\mathbf{x})d^3\mathbf{x},$$

$$F(\mathbf{x})=f(\rho(\mathbf{x}))+\frac{1}{2}\int_{r>d}U(r)[\rho(\mathbf{x}+\mathbf{r})-\rho(\mathbf{x})]d^3\mathbf{r}, \quad (1)$$

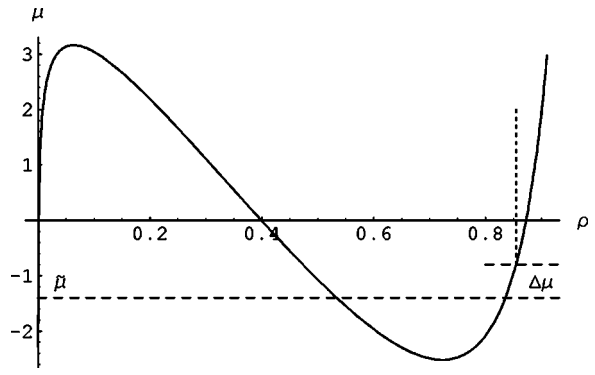

FIG. 1. The equilibrium curve $\mu=g(\rho)$ computed using Eq. (A6) with $\beta=9$. The value of the chemical potential at Maxwell construction μ_0 is taken as the zero level. The shift of chemical potential due to proximity of the interfaces $\tilde{\mu}$ and the dynamic shift $\Delta\mu$ near the cusp are indicated by dashed lines. The dotted line indicates the liquid density depletion.

where $f(\rho)$ is free energy per particle of a homogeneous fluid and $U(r)$ is an isotropic pair interaction kernel with a short-scale cutoff d. The chemical potential $\mu=\delta\mathcal{F}/\delta\rho$ enters the respective Euler-Lagrange equation obtained by minimizing the grand ensemble thermodynamic potential $\Phi=\mathcal{F}-\mu\int\rho\, d^3\mathbf{x}$, which defines the equilibrium density distribution $\rho(\mathbf{x})$:

$$g(\rho)-\mu+\int_{r>d}U(r)[\rho(\mathbf{x}+\mathbf{r})-\rho(\mathbf{x})]d^3\mathbf{r}=0, \quad (2)$$

where $g(\rho)=d[\rho f(\rho)]/d\rho$. The function $\rho[f(\rho)-\mu]$ should have two minima $\rho_s^{\pm}$ corresponding to two stable uniform equilibrium states of higher and lower density (liquid and vapor).

A typical function $g(\rho)$ defining the dependence $\mu(\rho)$ for a homogeneous fluid is shown in Fig. 1. Equilibrium between the two homogeneous states, $\rho=\rho_s^{\pm}$ is fixed by the Maxwell condition

$$\mu_0=\frac{\rho_s^+f(\rho_s^+)-\rho_s^-f(\rho_s^-)}{\rho_s^+-\rho_s^-}, \quad (3)$$

which defines, together with $\mu_0=g(\rho_s^{\pm})$, the equilibrium chemical potential μ_0 and both equilibrium densities.

The equation for density distribution near a flat boundary normal to the x axis is obtained by assuming ρ to be constant in each lateral plane and integrating Eq. (1) in the lateral directions. This yields the free energy per unit area, or surface tension,

$$\gamma=\int_{-\infty}^{\infty}\rho(x)[f(\rho)-\mu]dx + \frac{1}{2}\int_{-\infty}^{\infty}\rho(x)dx\int_{-\infty}^{\infty}Q(\xi)[\rho(x+\xi)-\rho(x)]d\xi. \quad (4)$$

The interfacial energy is contributed both by deviations from the equilibrium density levels in the transitional region and by the distortion energy localized there. The 1D interaction

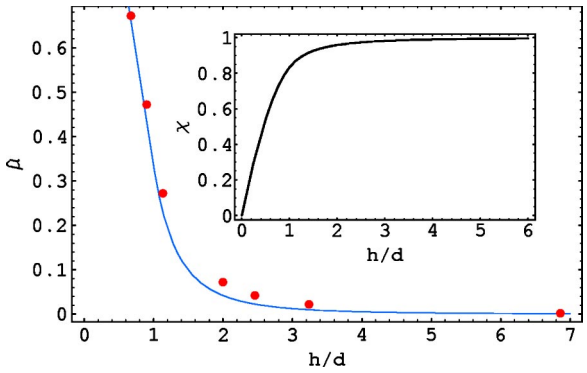

FIG. 2. The dependence of the dimensionless conjoining potential $\hat{\mu}$ on separation h. The dots denote the results of 1D density functional computation [18] with a shift of h adjusted to fit Eq. (8), as shown by the solid line. Inset: the function $\chi(h)$, Eq. (7).

kernel $Q(x)$ lumps intermolecular interaction between the layers $x=$const. It is computed by lateral integration, as described for the particular case of a van der Waals fluid in Appendix A.

The respective 1D Euler-Lagrange equation, replacing Eq. (2), is

$$g(\rho(x)) - \mu + \int_{-\infty}^{\infty} Q(\xi)[\rho(x+\xi) - \rho(x)]d\xi = 0. \qquad (5)$$

A stationary solution of Eq. (5) exists at a certain value of μ shifted downward from the Maxwell construction level μ_0, as shown by the dashed line in Fig. 1. The shift $\tilde{\mu}=\mu-\mu_0$ is the *conjoining potential* expressing the interaction of two identical flat interfaces.

The problem is solved numerically by fixing some trial value of μ and solving Eq. (5) iteratively to find a stationary profile $\rho(x)$ at this value [18]. The computation results for a van der Waals fluid (see Appendix A) using Eq. (A6) with $\beta=9$ are shown by dots in Fig. 2. To facilitate comparison with sharp-interface hydrodynamic theory, the conjoining potential is plotted against the nominal gap width h defined as

$$h = \frac{1}{\rho_s^+ - \rho_s^-}\int_{-\infty}^{\infty}(\rho - \rho_s^-)dx. \qquad (6)$$

The interfacial thickness, which lies far from the critical point in the nanometer range, is negligible compared to all relevant hydrodynamic lengths except the gap between two interfaces near the cusp. The correspondence between the surface tension of a sharp liquid-gas interface dependent on the gap width and the interfacial energy of a diffuse interface computed in the framework of density functional theory as a function of the nominal gap thickness can be established through a sharp-interface approximation of Eq. (4).

Straightforward computation using Eq. (4) with the van der Waals interaction kernel (A4) and the respective function $f(\rho)$, Eq. (A2), gives the following dependence of surface tension on the separation h:

$$\chi = \frac{\gamma}{\gamma_0} = \begin{cases} \frac{4}{3}\frac{h}{d} - \frac{1}{2}\left(\frac{h}{d}\right)^2 & \text{at } h \leqslant d, \\ 1 - \frac{1}{6}\left(\frac{d}{h}\right)^2 & \text{at } h \geqslant d. \end{cases} \qquad (7)$$

The respective sharp-interface approximation of the conjoining potential is obtained by differentiating Eq. (7) with respect to h:

$$\hat{\mu} = \tilde{\mu}(\rho_s^+ - \rho_s^-)\frac{d}{\gamma_0} = \frac{d\chi}{dh} = \begin{cases} \frac{4}{3} - \frac{h}{d} & \text{at } h \leqslant d, \\ \frac{1}{3}\left(\frac{d}{h}\right)^3 & \text{at } h \geqslant d. \end{cases} \qquad (8)$$

The curve $\hat{\mu}(h)$ expressing this dependence well fits the numerical results obtained by solving Eq. (A5) if the gap thickness is shifted by a certain value h_0 equal to ≈ 1.39 in this particular computation (Fig. 2).

A shift is necessary because no stationary solution can exist below a certain value of h, as defined by Eq. (6), which corresponds to a critical size required for nucleation of a critical 1D "bubble." By applying this shift, we assume that the nominal gap between sharp hydrodynamic interfaces is defined as the excess over this critical thickness. This fine distinction does not affect the geometry of the flow in the liquid domain, which is characterized by much larger length scales.

When the dependence $\chi(h)$ obtained for two flat and parallel interfaces is applied to the cusped interface, geometrical corrections are negligible. Indeed, close to the cusp tip [see Fig. 3(a)], the interface can be approximated as $x = y^{3/2}L^{-1/2}$, where L is the characteristic length scale of the outer flow. When the gap $h(y)=2x(y)=O(d)$, the slope $x'(y) \propto (y/L)^{1/2} \propto (d/L)^{1/3}$ is very small and the respective correction to the surface tension can be neglected. Likewise, the curvature radius is estimated as $\kappa^{-1} \approx 1/x''(y) \propto (yL)^{1/2} \propto L^{2/3}d^{1/3} \gg d$, so that curvature corrections are negligible higher-order quantities. We shall further use the simple expressions (7) and (8) bearing in mind that, provided the condition $\gamma(0)=0$ holds, the results are not significantly altered by the detailed form of the dependence of surface tension on separation.

III. HYDRODYNAMIC SOLUTION

Given a dependence $\chi(h)$, one can apply the powerful apparatus of hydrodynamic theory [10]. The hydrodynamic solution for the Stokes flow driven by a vortex dipole with the strength u_0 located at the point $y=-1$ in the plane $z=x+iy$ is found [10] by conformal transformation $z(\zeta)$ projecting the region occupied by the viscous liquid into the unit circle $\zeta=e^{i\theta}$ with the dipole source at its center. The applicable transformation is

$$z = a(\zeta + i) + i(1+a)\frac{\zeta - i}{\zeta + i}, \qquad (9)$$

dependent on a single parameter a; the interface is concave at $a<0$, and is non-self-intersecting at $a>-1/3$. Both infinitely removed points at the interface are projected onto the point $\theta=-\pi/2$. A cusp is formed at the point $z=-\frac{2}{3}i$ (projected onto $\theta=\pi/2$) when $a=-1/3$ [see Fig. 3(b)].

The tangential velocity on the interface, parametrized by the angle θ on the unit circle, is (see Appendix B for more detail)

$$u(e^{i\theta}) = -|z'(e^{i\theta})|\cos\theta\left[\frac{4u_0}{a(2+3a)^2} + \frac{1}{4\pi\eta}\int_0^{2\pi}\frac{\gamma(\vartheta)d\vartheta}{|z'(e^{i\vartheta})|(\sin\vartheta-\sin\theta)}\right], \quad (10)$$

where the principal value of the singular integral should be taken. Velocity should vanish at spatial infinity, i.e., at $\theta=-\pi/2$. This implies that the bracketed expression in Eq. (10) should vanish, yielding the relation between the parameter a and the capillary number $\mathrm{Ca}=u_0\eta/\gamma_0$

$$\mathrm{Ca} = \frac{a(2+3a)^2}{8\pi}\int_{-\pi/2}^{\pi/2}\frac{\chi(\vartheta)d\vartheta}{|z'(e^{i\vartheta})|(\sin\vartheta+1)}. \quad (11)$$

The integral in Eq. (11) diverges at $a=-1/3$, $\chi=1$, but remains finite when the surface tension vanishes at $\vartheta=\pi/2$. Using Eq. (7), the integral in Eq. (11) is computed analytically by separating it into two parts, inner and outer, joined at some angle $\vartheta=\pi/2-\Theta$, where $d\ll\Theta\ll1$. In the outer region $\vartheta>\Theta$, χ is set to unity, yielding (at $a=-1/3$) $\mathrm{Ca}^{\mathrm{out}}=(16\pi)^{-1}\ln(8/\Theta)$. In the inner region $\vartheta<\Theta$, the denominator is approximated as $|z'(e^{i\vartheta})|(\sin\vartheta+1)\approx\vartheta/3$. The computation yields a logarithmic divergence at $\Theta\to\infty$ canceling with the matching divergence of the outer integral upon summation: $\mathrm{Ca}^{\mathrm{in}}=(16\pi)^{-1}\ln(q\Theta)$, where q is a number dependent on the chosen dependence $\chi(\vartheta)$; q is finite, provided $\chi(\pi/2)=0$. The result is $\mathrm{Ca}=\mathrm{Ca}^{\mathrm{in}}+\mathrm{Ca}^{\mathrm{out}}=(16\pi)^{-1}\ln 8q$. Since the decrease of surface tension is felt only very close to the cusp, one can use the approximate expression for separation $h=\frac{1}{6}(\pi/2-\vartheta)^3$. Using this together with Eq. (7) to compute $\mathrm{Ca}^{\mathrm{in}}$ yields $q=(e/6d)^{1/3}$, so that

$$\mathrm{Ca} = \mathrm{Ca}^{\mathrm{in}} + \mathrm{Ca}^{\mathrm{out}} = \frac{1}{48\pi}\left(1+\ln\frac{256}{3d}\right). \quad (12)$$

We see that the cusp is indeed formed at a finite (and not very large) Ca, e.g., $\mathrm{Ca}\approx0.158$ at $d=10^{-8}$; this value is in fact *lower* than Ca in the solution with $\gamma=$const with the tip curvature $\kappa=d^{-1}$ (see Fig. 4), so that formal rounding up of the cusp has no physical significance under these conditions.

The interfacial velocity defined by Eq. (10) is computed in the same way, although care should be taken to apply different approximations near and far from the cusp tip and matching the results. Far from the tip, the solution is practically indistinguishable from a solution with $\gamma=$const and the same value of Ca, but in the immediate vicinity of the tip the behavior is qualitatively different (Fig. 5): the stagnation

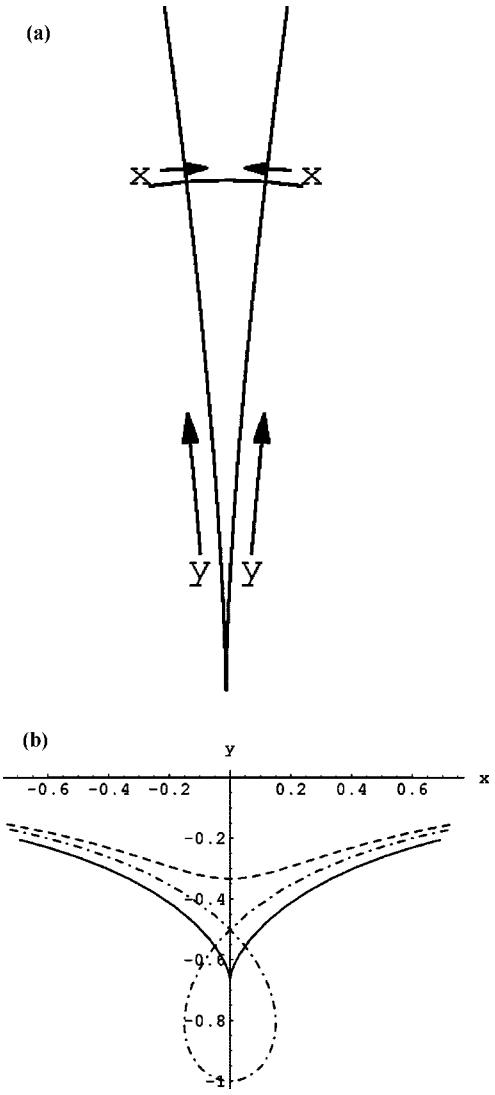

FIG. 3. (a) The shape of the interface near the cusp. Arrows show the local directions of the x and y axes in a coordinate system aligned with the interface. (b) The interfacial shapes defined by Eq. (10) with $a=-1/3$ (solid curve), $a>-1/3$ (dashed curve), and $a<-1/3$ (dash-dotted curve).

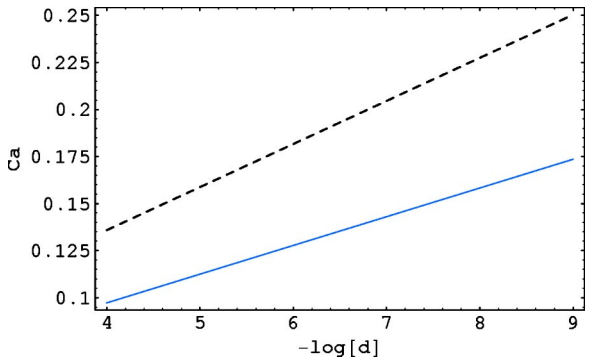

FIG. 4. The dependence of the capillary number at the cusp point on the molecular cutoff length d expressed in the outer flow units. The dashed line shows the capillary number for the hydrodynamic solution with the tip curvature radius d.

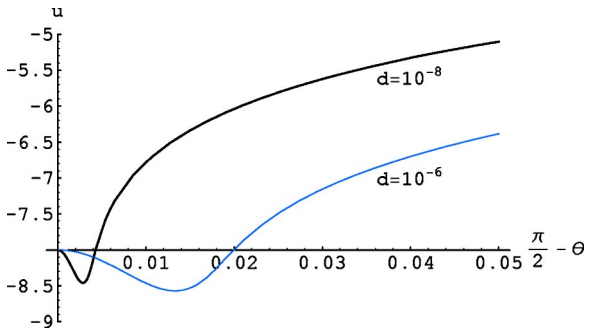

FIG. 5. The interfacial velocity near the cusp at $d=10^{-8}$ and $d=10^{-6}$.

point disappears, and the downward velocity is finite at the cusp tip.

At higher values of Ca, the transform (9) can be modified then by including a cubic term:

$$z = a(\zeta + i) + b(\zeta + i)^3 + i(1 + a - b)\frac{\zeta - i}{\zeta + i}. \tag{13}$$

A fifth-order singularity attained at $a=8/19$, $b=1/95$ corresponds to a still deeper and narrower tip formed at higher values of Ca. This can be continued by adding higher-order terms and pushing the interfacial singularity still closer to the vortex dipole. All this is, however, a mere formal exercise, as the gap width drops near higher-order singularities well below molecular scale. It is more likely that the value of Ca corresponding to $a=-1/3$ can be identified with the limit of air entrainment. Transverse instability of the air sheet should be facilitated near this limit by conjoining interaction of the two interfaces.

IV. INTERPHASE TRANSPORT

After establishing that the flow velocity is finite near the tip, we can shift attention to gas flow and vapor-liquid equilibrium in the narrow gap. Relaxation of density toward equilibrium is constrained by the mass conservation law

$$\partial_t \rho = -\ \boldsymbol{\nabla} \cdot \mathbf{j}. \tag{14}$$

If deviations from equilibrium are weak, the flux $\mathbf{j}$ can be assumed to be proportional to the gradient of the chemical potential:

$$\mathbf{j} = -\Gamma(\rho)\, \boldsymbol{\nabla}\, \mu, \tag{15}$$

where Γ is a mobility coefficient, generally dependent on ρ. This formulation ensures a monotonic approach to equilibrium. Equations (14) and (15) combine to the generalized Cahn-Hilliard equation

$$\partial_t \rho = \boldsymbol{\nabla} \cdot [\Gamma(\rho)\, \boldsymbol{\nabla}\, \mu]. \tag{16}$$

Relations between the condensation flux j, normal displacement velocity of the interface c, and drop of chemical potential across the interface $\Delta\mu$ can be obtained by solving Eqs. (5) and (16) in the thin interface approximation:

$$j = \rho_s^+ c = D^- \partial_n^0 \rho_s^- - D^+ \partial_n^0 \rho_s^+, \tag{17}$$

$$\Delta\mu = c \int_{-\infty}^{\infty} \rho_0'(x) dx \int_0^x \frac{\rho_0(x')}{\Gamma(\rho_0(\xi))} d\xi \equiv \frac{c}{\lambda}. \tag{18}$$

Here $D^{\pm}=\Gamma(\rho_s^{\pm})g'(\rho_s^{\pm})$ are the diffusivities in the liquid and gas phases, λ is the effective mobility, and ρ_s^- is assumed negligible compared to ρ_s^+. These relations should be used as boundary conditions at the interface matching far field solutions in the liquid and gas phases.

The derivation of Eqs. (17) and (18) given in Appendix C follows the general scheme worked out in phase field theory of phase transitions [19]. The reader can omit details of the derivation, taking note that Eq. (17) is just the mass conservation condition for a moving interface, while Eq. (18) can be viewed, disregarding its middle part, as a linear relation between $\Delta\mu$ and c with an adjustable proportionality constant λ. This constant is in fact not independent but is expressed through mobilities, but this formula is not very useful practically due to the lack of data on the dependence $\Gamma(\rho)$. The upper estimate is $\lambda \propto \Gamma_l/(d\rho_s^+) \propto D^+/(dT) \approx 10^{21}$ sec m^{-1} kg^{-1}, but this value may be depressed considerably by an Arrhenius factor. It is also shown in Appendix C that Eq. (18) should be corrected when the mobility Γ strongly depends on density.

The Galilean invariant extension of Eq. (16) is

$$\partial_t \rho + \boldsymbol{\nabla} \cdot (v\rho) = -\boldsymbol{\nabla} \cdot [\Gamma(\rho)\, \boldsymbol{\nabla}\, \mu]. \tag{19}$$

This is a material balance equation, which reduces to the continuity equation outside thin interfacial layers. A conceptual difficulty arises, however, since Eq. (19) contains both diffusional and advective fluxes, which cannot be separated in a unique way in a one-component fluid. In the case under study, this separation is natural, since the flow is determined by the macroscopic solution obtained in Sec. III, while the diffusional transport is minute and its contribution to the momentum balance is negligible. Thus, Eqs. (17) and (18) can be retained to define the flux in a local Galilean frame moving with the velocity determined by the available hydrodynamic solution.

In the outer (bulk) regions the distortion term in Eq. (5) can be neglected, and the density closely approaches one of the alternative equilibria $\rho_s^{\pm}$, while deviation of the chemical potential μ from the Maxwell construction can be approximated as $\mu-\mu_s=g'(\rho_s^{\pm})(\rho-\rho_s^{\pm})$. Thus, Eq. (16) reduces to a linear convective-diffusion equation

$$\partial_t \rho^{\pm} + \boldsymbol{\nabla} \cdot (\mathbf{v}\rho) = D^{\pm} \nabla^2 \rho^{\pm}. \tag{20}$$

The potential difference driving the interphase transport is $\Delta\mu=g(\rho_s^-)-\tilde{\mu}$ (see Fig. 1), where $\tilde{\mu}$ is the shift of equilibrium chemical potential in a narrow gap estimated by Eq. (8). This reduces the interphase transport problem to solving the far field convective diffusion equations in both phases using Eqs. (17) and (18) as matching conditions. The problem is additionally simplified in our case, since the limiting stage largely determining the shift of chemical potential is removal of an inert component (air) advected into the narrow cusp interstice.

V. TRANSPORT IN GAS AND LIQUID PHASES

In the gas phase within the cusp, density changes in the transverse direction can be neglected, and the applicable equation for the vapor density is

$$\partial_y(D^- h\partial_y\rho^- - uh\rho^-) - 2j(y) = 0, \tag{21}$$

where $j(y)$ is the local condensation flux at each of the symmetric interfaces, and u is the interfacial velocity given by the above hydrodynamic solution, which is almost constant at relevant distances from the cusp tip. The transport of the inert component is governed by a similar equation, but with a vanishing total flux. Assuming the gas pressure p to be constant (which is justified by the absence of transverse gradients and negligible interfacial curvature in the cusp), we have

$$D^-\partial_y\rho^- + u(p/T - \rho^-) = 0, \tag{22}$$

where T is temperature. This can be used back in Eq. (21) to compute the condensation flux $j(y) = -(up/2T)h'(y)$. On the other hand, it follows from the material balance for the two interfaces on the sides of the cusp that

$$-c\rho_s^+ = j(y) = -\frac{up}{2T}h'(y) = \left(\frac{3}{2}\right)^{3/2}\frac{up\sqrt{h}}{2T}. \tag{23}$$

Using Eqs. (18) and (23) can estimate the gap width at which the interaction of the interfaces becomes sufficient to drive this condensation flux. Since the flux is minute, this distance turns out to be much larger than the molecular scale. The estimate is given by

$$\left(\frac{d}{h}\right)^{7/2} \approx \frac{\rho_s^-}{\rho_s^+}\frac{u\sqrt{d}}{\lambda T}, \tag{24}$$

yielding a gap width about 10^{-7} m. The corresponding length of the condensation zone from which air should be removed by diffusion is in a rather macroscopic range of tens of micrometers. The total condensation flux obtained by integrating Eq. (23) over this length is about 10^{16} m^{-2} sec^{-1}. This is quite minute on a macroscopic scale, as the effective condensation velocity c obtained by dividing the above value by ρ_s^+ is about 10^{-12} m/sec, and should not affect significantly the shape of the cusp.

In the liquid phase, one has to solve the convective diffusion equation

$$D^+\nabla^2\rho^+ - \mathbf{u}\cdot\boldsymbol{\nabla}\rho^+ = 0. \tag{25}$$

Near the cusp, the flow velocity $\mathbf{u}$ can be assumed to be constant and directed down the y axis (parallel to the cusp). Small deviations from equilibrium liquid density are caused by the lowering of chemical potential, as seen in Fig. 1. The solution far downstream is

$$\tilde{\rho}^+ \propto \frac{\Delta\mu}{g'(\rho_s^+)}\exp\left(\frac{uy}{2D}\right)K_0\left(\frac{uy}{2D}\right) \approx \frac{c}{\lambda g'(\rho_s^+)}\left(\frac{uy}{2D}\right)^{-1/2}. \tag{26}$$

Although the source of density depletion is very weak, it decays extremely slowly downstream, creating a relaxation effect similar to that envisaged by Shikhmurzaev [13].

VI. CONCLUSIONS

The contest between a true cusp singularity and a stagnation point is resolved by mesoscopic theory including molecular interactions in favor of the cusp, since the velocity at the tip computed in Sec. III remains finite, although the distinction of shapes is blurred due to the diffuse character of the interface. The theory presented here does not overlap with that of Eggers [12] operating on much larger scales. Although condensation does relieve the air pressure through diffusion, it becomes significant only at mesoscopic distances from the tip, and viscous pressure may accumulate at larger scales causing entrainment of macroscopic bubbles. The latter problem still remains unresolved, since the dependence of the critical capillary number of air entrainment on the viscosity ratio detected experimentally [20] is much weaker than that predicted theoretically [12]. An experimental test of the role of condensation (acting as a last-ditch defense against entrainment) would require testing fluids with different volatilities as well as viscosities.

In a more general context, the principal message of this communication is the importance of interphase transport and flow induced by molecular interactions in the vicinity of interfacial singularities. This may be relevant in various situations involving close approach of surfaces, such as coalescence failure, dewetting, or spreading. A specific phenomenon, which, to this author's knowledge, has never been described before, is a kind of Marangoni flow induced by the proximity of interfaces, rather than by composition of temperature changes. Both Marangoni flow and interphase transport are identified in the sharp-interface limit of the diffuse interface theory that connects interactions on the molecular scale to macroscopic hydrodynamic theory.

ACKNOWLEDGMENT

This research has been supported by Israel Science Foundation (Grant No. 55/02).

APPENDIX A: DENSITY FUNCTIONAL THEORY FOR A VAN DER WAALS FLUID

This appendix presents a simple example of derivation of a particular form of the function $f(\rho)$ and 1D interaction kernel $Q(x)$ using the modified Lennard-Jones potential with hard-core repulsion

$$U = \begin{cases} -Ar^{-6} & (r > d), \\ \infty & (r < d), \end{cases} \tag{A1}$$

where d is the nominal hard-core molecular diameter. Using this interaction kernel, the free energy per particle of a homogeneous van der Waals fluid is computed as

$$f(\rho,T) = T\ln\frac{\rho}{1-b\rho} - a\rho, \tag{A2}$$

where T is the temperature, $b = \frac{2}{3}\pi d^3$ is the excluded volume, and

$$a = -2\pi \int_d^\infty U(r) r^2 dr = \frac{2\pi A}{3d^3}. \tag{A3}$$

The 1D interaction kernel $Q(x)$ is computed using as an integration variable the squared distance $q=r^2=\xi^2+x^2$, where ξ is the radial distance in the lateral plane. Taking note that the lower integration limit for q is $q_0=x^2$ at $|x|>d$, $q_0=d^2$ at $|x|\leqslant d$, we compute

$$Q(x) = -\pi A \int_{q_0}^\infty q^{-3} dq = \begin{cases} -\frac{1}{2}\pi A x^{-4} & \text{at} \quad |x|>d, \\ -\frac{1}{2}\pi A d^{-4} & \text{at} \quad |x|<d. \end{cases} \tag{A4}$$

The dimensionless form of Eq. (5) obtained by plugging in there Eqs. (A2) and (A4) is

$$g(\rho) - \mu + \frac{3}{4}\beta \int_{-\infty}^\infty \hat{Q}(\xi)[\rho(x+\xi)-\rho(x)]d\xi = 0, \tag{A5}$$

$$g(\rho) = \frac{1}{1-\rho(x)} - \ln\left(\frac{1}{\rho(x)} - 1\right) - 2\beta\rho(x). \tag{A6}$$

Here the length is scaled by the nominal molecular cutoff diameter d, the density by b^{-1}, and the chemical potential by temperature T; the interaction kernel is $\hat{Q}(x)=-x^{-4}$ at $x>1$, $\hat{Q}(x)=-1$ at $x<1$, and the only remaining dimensionless parameter is the rescaled inverse temperature $\beta=a/(bT)$.

APPENDIX B: COMPLEX REPRESENTATION OF THE FLOW FIELD

This appendix outlines the solution of the hydrodynamic free surface problem via conformal transformation [10]. A stationary flow field $\boldsymbol{u}(x,y)$ of a viscous incompressible liquid and a pressure field p satisfy the Stokes and continuity equations

$$\boldsymbol{\nabla} p = \eta \nabla^2 \mathbf{u}, \quad \boldsymbol{\nabla}\cdot\mathbf{u} = 0. \tag{B1}$$

A 2D flow field $\mathrm{u}(x,y)=(u_1,u_2)=(\psi_y,-\psi_x)$ is defined through the stream function $\psi(x,y)$ solving the biharmonic equation $\nabla^4\psi=0$. We consider a semi-infinite domain bounded by a liquid-gas interface Γ; the gas phase is assumed to be inviscid. The boundary conditions on Γ are

$$\mathbf{u}\cdot\mathbf{n} = 0, \quad \mathbf{n}\cdot\boldsymbol{\sigma}\cdot\mathbf{n} = \gamma\kappa,$$

$$(\mathbf{I}-\mathbf{nn})\cdot\boldsymbol{\sigma}\cdot\mathbf{n} = \boldsymbol{\nabla}\gamma, \tag{B2}$$

where $\mathbf{n}$ is the normal to the interface, I is the unity tensor, γ is the surface tension, and κ is the interfacial curvature. The elements σ_{ij} of the stress tensor $\boldsymbol{\sigma}$ can be defined through an Airy stress function $\phi(x,y)$ satisfying $p=\eta\nabla^2\phi$:

$$\sigma_{11} = -2\eta\phi_{yy}, \quad \sigma_{22} = -2\eta\phi_{xx}, \quad \sigma_{12}=\sigma_{21}=2\eta\phi_{xy}. \tag{B3}$$

The kinematic boundary condition in Eq. (B2) reduces to $\psi=\mathrm{const}=0$, while the normal and tangential stress boundary conditions are expressed in terms of ϕ as

$$\phi = 0, \quad \mathbf{n}\cdot\boldsymbol{\nabla}\phi = \gamma/(2\eta). \tag{B4}$$

In the complex representation, the flow is characterized by the complex potential $w(z,\bar{z})=\phi+i\psi$. A general biharmonic function is expressed using the Goursat representation as $w=w_0+\bar{z}w_1$, where w_0, w_1 are harmonic functions of the complex variable $z=x+iy$; the over bar denotes the complex conjugate. The two functions w_0, w_1 completely specify the flow field [21]

$$u = u_1 + iu_2 = \overline{w_0'(z)} + z\overline{w_1'(z)} - w_1(z). \tag{B5}$$

The kinematic and normal stress boundary conditions reduce to a single complex condition

$$w_0(z) + \bar{z}w_1(z) = 0. \tag{B6}$$

The tangential stress boundary condition becomes

$$\mathrm{Im}\left[w_1(z)\frac{\partial\bar{z}}{\partial s}\right] = \frac{\gamma}{4\eta}, \tag{B7}$$

where s is the arclength on Γ.

Following the conformal transformation $z(\zeta)$ mapping the interface on the unit circle $|\zeta|=1$, the boundary condition (B6), yields the relation between the two unknown functions $W_k(\zeta)=w_k(z(\zeta))$, $k=0, 1$:

$$W_0(\zeta) = -\overline{z}(\zeta)W_1(\zeta) \mathrm{on} |\zeta| = 1. \tag{B8}$$

Using the relation valid on the unit circle,

$$\frac{dz}{ds} = i\zeta\frac{z'(\zeta)}{|z'(\zeta)|} = \left[\frac{d\bar{z}}{ds}\right]^{-1}, \tag{B9}$$

the remaining boundary condition (B7) reduces to the equation for $W_1(\zeta)$:

$$\mathrm{Re}\left[\frac{W_1(\zeta)}{\zeta z'(\zeta)}\right] = -\frac{\gamma}{4\eta|z'(\zeta)|}. \tag{B10}$$

The dependence on the dipole strength is established through the asymptotics at $\zeta\to 0$:

$$W_0(\zeta) \propto \frac{iu_0}{\zeta z'(0)}, \quad W_1(\zeta) \propto -\frac{iu_0}{az'(0)}. \tag{B11}$$

The solution is found by using analytic continuation of the condition (B10) away from the unit circle and computing W_1 with the help of the Poisson formula. In order to cancel the singularity at the origin, Eq. (B10) is modified to

$$\mathrm{Re}\left[\frac{W_1(\zeta)}{\zeta z'(\zeta)} - \frac{W_1(0)}{\zeta z'(0)}(1-\zeta^2)\right] = -\frac{\gamma}{4\eta|z'(\zeta)|}. \tag{B12}$$

The Poisson formula yields then

$$W_1(\zeta) = \frac{z'(\zeta)}{z'(0)} W_1(0)(1-\zeta^2) - \frac{\gamma\zeta z'(\zeta)}{8i\pi\eta} \oint \frac{(\xi+\zeta)d\xi}{|z'(\zeta)|(\xi-\zeta)\xi}. \tag{B13}$$

The expression (10) for the tangential velocity on the interface is obtained from this general expression using Eqs. (9), (B5), (B8), and (B11).

APPENDIX C: COMPUTATION OF THE CONDENSATION FLUX

The characteristic width of a diffuse interface is of the same order of magnitude as the molecular cutoff length d, and increases to larger (mesoscopic) distances only close to the critical point. Across this thin layer, the fluid density switches between the two alternative values corresponding to the same constant value of chemical potential. The latter serves as a bias parameter that shifts the equilibrium in favor of one of the phases. Under nonequilibrium conditions, the chemical potential varies on a longer scale L that is be determined by the geometry of the system. Problems of this kind, containing a small parameter $\epsilon = d/L$, should be solved by matching expansions in ϵ in regions characterized by two widely separated scales: the *inner* region localized at the interface, and the *outer* region spreading out to the bulk of both alternative phases. This approach is suitable to track slow motion of the interphase boundary at times far exceeding the characteristic relaxation time to a stationary profile of the order parameter in the interfacial layer.

In the inner region, the characteristic scale along the axis x normal to the nominal front position is the short scale d, while the coordinate y parallel to the interface is scaled by L. Inasmuch as the interfacial layer is assumed to be locally close to equilibrium, the interface is expected to move under the influence of long-scale changes of the chemical potential. Therefore the propagation speed should be measurable on a long scale, so that the "Péclet number" $\mathrm{Pe} = cL/D$ based on the long length scale L and a typical value of the diffusivity should be at most of $O(1)$. In accordance with this scaling, we express the propagation speed as ϵc. Retaining the terms up to the first order, we rewrite Eq. (16) as

$$d_x[\Gamma(\rho)\mu'(x)] + \epsilon c\rho'(x) = 0. \tag{C1}$$

This equation is solved together with Eq. (5).

The solution of the inner equations is sought for as an expansion in ϵ:

$$\rho = \rho_0 + \epsilon\rho_1 + \cdots, \quad \mu = \mu_0 + \epsilon\mu_1 + \cdots. \tag{C2}$$

In the zero order, Eq. (C1) reduces to $\mu_0''(x) = 0$, while the zero order density profile $\rho_0(x)$ is a stationary front verifying Eq. (5) that exists when μ_0 is the equilibrium chemical potential defined by Eq. (3). Formally, one could still add to μ_0 a linear term, but this would be incompatible with matching conditions when propagation is slow. Thus, the variable part of μ is restricted in the interfacial layer to $O(\epsilon)$.

In the first order, Eq. (C1) reduces to

$$d_x[\Gamma(\rho_0)\mu_1'(x)] + c\rho_0'(x) = 0. \tag{C3}$$

The solutions of the inner and outer equations should be matched at a distance from the front that is large on the inner but small on the outer scale; the result must be independent of a precise matching position within this range. The matching conditions are

$$\lim_{x\to\pm\infty} \mu_1'(x) = \partial_n^0 \mu^{\pm}, \tag{C4}$$

where ∂_n is the derivative along the normal $\boldsymbol{n}$ (directed, by convention, in the same way as the x axis) and the superscript 0 indicates the inner limit of the outer solution computed near the interface.

Integrating Eq. (C3) and using Eq. (C4) yields

$$c(\rho^+ - \rho^-) = -\Gamma(\rho^+)\partial_n^0\mu^+ + \Gamma(\rho^-)\partial_n^0\mu^- \equiv j^+ - j^-. \tag{C5}$$

The right-hand side of Eq. (C5) is the difference of the fluxes on the two sides; thus, this condition defines the speed of the local interface displacement required to ensure the mass conservation. Since the variable part of μ is restricted in the interfacial layer to $O(\epsilon)$, the values $\rho^{\pm}$ of the density in the matching regions may deviate from the equilibrium values $\rho_s^{\pm}(\mu_s)$, satisfying $\mu_s = g(\rho_s^{\pm})$ by no more than $O(\epsilon)$. Using again a linearization of $g(\rho)$, the mass conservation condition (C5) can be rewritten as

$$c = \frac{D_s^+\partial_n^0\rho^- - D_s^-\partial_n^0\rho^+}{\rho_s^+ - \rho_s^-}, \tag{C6}$$

which reduces to Eq. (17) when $\rho_s^- = \rho_s^-$ is neglected.

It remains to determine the first-order correction to the interfacial chemical potential and the related values of density $\rho^{\pm}$ at the matching locations on both sides of the interface. For this purpose, Eq. (C3) is integrated twice to yield

$$\mu_1(x) = \overline{\mu_1} + \int_0^x \frac{j_1 - c\rho_0(x)}{\Gamma(\rho_0(x))}dx, \tag{C7}$$

where $\overline{\mu_1} = \mu_1(0)$ and j_1 are integration constants. The latter equals the flux through the interface, which is determined by the matching conditions (C4) yielding two equivalent expressions

$$j_1 = \Gamma(u^{\pm})\partial_n^0\mu^{\pm} + c\rho^{\pm} = c\rho^{\pm} - j^{\pm} = \frac{j^+\rho_s^- - j^-\rho_s^+}{\rho_s^+ - \rho_s^-}. \tag{C8}$$

The flux j_1 vanishes for a single interface viewed in the comoving frame.

The first-order expansion of Eq. (5),

$$g'(\rho_0)\rho_1 - \mu_1 + \int_{-\infty}^{\infty} Q(\xi)[\rho_1(x+\xi) - \rho_1(x)]d\xi = 0, \tag{C9}$$

is a linear inhomogeneous equation of a general form $\mathcal{H}\rho_1 + \Psi = 0$ with an integral linear operator $\mathcal{H}$ and an inhomogeneity $\Psi = -\mu_1$. By the Fredholm alternative, the solvability condition of this equation is orthogonality of Ψ to the neutrally stable eigenmode of $\mathcal{H}$. The latter is determined by translational symmetry of the system and coincides with the derivative $\rho_0'(x)$. Using Eq. (C7) yields

$$\overline{\mu_1}(\rho_s^+ - \rho_s^-) = -j_1\mathcal{J}_0 + c\mathcal{J}_1, \tag{C10}$$

$$\mathcal{J}_k = \int_{-\infty}^{\infty} \rho_0'(x)dx \int_0^x \frac{\rho_0^k(\xi)}{\Gamma(\rho_0(\xi))}d\xi = \int_0^{\infty} \frac{\rho_0^k(\xi)[\rho_s^+ - \rho(\xi)]}{\Gamma(\rho_0(\xi))}d\xi - \int_{-\infty}^{0} \frac{\rho_0^k(\xi)[\rho(\xi) - \rho_s^-]}{\Gamma(\rho_0(\xi))}d\xi \equiv \mathcal{J}_k^+ - \mathcal{J}_k^-. \tag{C11}$$

The limit of the inner solution (C7) at $x \to \pm\infty$ is

$$\lim_{x\to\pm\infty} \mu_1(x) = \overline{\mu_1} + c\mathcal{J}_0^{\pm} - j^{\pm}\mathcal{K}^{\pm} + x\partial_n^0\mu^{\pm}, \tag{C12}$$

where we have used Eq. (C8) and separated the converging integrals $\mathcal{J}_0^{\pm}$, defined by Eq. (C11), and

$$\mathcal{K}^{\pm} = \int_0^{\pm\infty} \left[\frac{1}{\Gamma(\rho_0(x))} - \frac{1}{\Gamma(\rho_s^{\pm})}\right]dx. \tag{C13}$$

On the other hand, the chemical potential in the outer regions close to the interface, i.e., at some distance along the normal $\boldsymbol{n}$, which is small when measured on the outer scale, is presented by expanding the outer solution in Taylor series as

$$\mu^{\pm} = \overline{\mu^{\pm}} + x\partial_n^0\mu^{\pm}. \tag{C14}$$

The last terms in Eqs. (C12) and (C14) match, and the remaining constant terms yield two matching conditions for computing $\overline{\mu^{\pm}}$:

$$\overline{\mu^{\pm}} - \mu_s = \overline{\mu_1} + c\mathcal{J}_0^{\pm} - j^{\pm}\mathcal{K}^{\pm}. \tag{C15}$$

The difference between the two values is

$$\Delta\mu = \mu^+ - \mu^- = c(\mathcal{J}_0^+ - \mathcal{J}_0^- - \rho_s^+\mathcal{K}^+ + \rho_s^-\mathcal{K}^-) + j_1(\mathcal{K}^+ - \mathcal{K}^-), \tag{C16}$$

where we have used Eq. (C8). Equation (18) is a simplified version of this expression neglecting the integrals $\mathcal{K}^{\pm}$ which are significant when the mobility Γ strongly depends on density.

[1] E.B. Dussan V., Annu. Rev. Fluid Mech. **11**, 371 (1979).
[2] P.G. de Gennes, Rev. Mod. Phys. **57**, 827 (1985).
[3] T.D. Blake and J.M. Haynes, J. Colloid Interface Sci. **30**, 421 (1969).
[4] L.M. Pismen and B.Y. Rubinstein, Langmuir **17**, 5265 (2001).
[5] Y.D. Shikhmurzaev, J. Fluid Mech. **334**, 211 (1997).
[6] D. Jacqmin, J. Fluid Mech. **402**, 57 (2000).
[7] L.M. Pismen and Y. Pomeau, Phys. Rev. E **62**, 2480 (2000).
[8] L.M. Pismen, Phys. Rev. E **64**, 021603 (2001).
[9] D.D. Joseph, J. Nelson, M. Renardy, and Y. Renardy, J. Fluid Mech. **223**, 383 (1991).
[10] J.-T. Jeong and H.K. Moffatt, J. Fluid Mech. **241**, 1 (1992).
[11] L.K. Antanovskii, Eur. J. Mech. B/Fluids **13**, 491 (1994).
[12] J. Eggers, Phys. Rev. Lett. **86**, 4290 (2001).
[13] Y.D. Shikhmurzaev, J. Fluid Mech. **359**, 313 (1998).
[14] J.D. van der Waals, Z. Phys. Chem., Stoechiom. Verwandtschaftsl. **13**, 657 (1894); English translation by J.S. Rowlinson, J. Stat. Phys. **20**, 197 (1979).
[15] D.M. Anderson, G.B. McFadden, and A.A. Wheeler, Annu. Rev. Fluid Mech. **30**, 139 (1998).
[16] J.W. Cahn and J.E. Hilliard, J. Chem. Phys. **31**, 688 (1959).
[17] S. Dietrich and M. Napiòrkowski, Phys. Rev. A **43**, 1861 (1991).
[18] A. Yochelis and L.M. Pismen (unpublished).
[19] A. Karma and W.-J. Rappel, Phys. Rev. E **57**, 4323 (1998).
[20] E. Lorenceau, F. Restagno, and D. Quéré, Phys. Rev. Lett. **90**, 184501 (2003).
[21] S. Richardson, J. Fluid Mech. **33**, 467 (1968).